An Overlapping Domain Decomposition Method for a 3D PEMFC Model

Cheng Wang[1], Mingyan He[1], Ziping Huang[2], and Pengtao Sun[3]

[1] Department of Mathematics, Tongji University, Shanghai, China
wangcheng@tongji.edu.cn hemingyan1985@yahoo.com.cn
[2] Chinese-German College, Tongji University, Shanghai, China huangziping@tongji.edu.cn
[3] Department of Mathematical Sciences, University of Nevada Las Vegas, 4505 Maryland Parkway, Las Vegas, NV 89154 pengtao.sun@unlv.edu

Summary. In this paper, an overlapping domain decomposition method is developed to simulate the water management of the polymer exchange membrane fuel cell on the local structured grids. Numerical experiments demonstrate that our methods are effective to deal with the simulation on the non-matching grids with low mass balance error.

1 Introduction

Polymer exchange membrane fuel cells (PEMFCs) have been used in a large number of industries worldwide because of their advantages such as low environmental impact, rapid start-up and high power density [15, 16]. The performance of fuel cell is affected by many factors, such as material parameters, operating conditions, different channel structures and so on [2, 9, 10].

For better performance, different structures for the anode and cathode gas channels are used in the PEMFC practical design. This asymmetrical structure can keep the balance of pressures on both sides of the membrane. Thus the water management in cathode can be improved and the duration of fuel cell can be prolonged. An unstructured grid partitioned by tetrahedra or triangles can be used for this asymmetrical fuel cell in single domain approach, but structured grids, such as hexahedron and quadrilateral, are easily implemented and have super convergence [1, 4, 14]. However, non-matching grids would be generated when partitioning with structured grids in numerical simulations. Besides, since oxygen reduction reaction occurs in cathode, the variation of physical quantities such as water concentration are more significant in cathode than in anode. So it is necessary for cathode to simulate these phenomena accurately by a refined grid. The objective of this paper is to provide an overlapping domain decomposition method for the simulation of a 3D single-phase PEMFC model with local structured grid in anode and cathode respectively.

R. Bank et al. (eds.), *Domain Decomposition Methods in Science and Engineering XX*, Lecture Notes in Computational Science and Engineering 91,
DOI 10.1007/978-3-642-35275-1_12,

1.1 Governing Equations

Based on [5, 16], a fundamental fuel cell model consists of five principles of conservation: mass, momentum, species, charge, and thermal energy. Typically the fuel cell is divided into seven subregions: the anode gas channel, anode gas diffusion layer (GDL), anode catalyst layer (CL), membrane, cathode gas channel, cathode GDL, and cathode CL. In the following we specifically focus our interests on mass, momentum conservation and water concentration arising in all seven subregions.

Flow equations. For flow field with velocity $\mathbf{u}$ and pressure P as unknowns, we have the following modified Navier-Stokes equations

$$\nabla \cdot (\rho \mathbf{u}) = 0, \tag{1}$$

$$\frac{1}{\varepsilon^2}\nabla \cdot (\rho \mathbf{u}\mathbf{u}) = -\nabla P + \nabla \cdot (\mu \nabla \mathbf{u}) + S_u, \tag{2}$$

where ε is porosity, ρ is density, and μ is effective viscosity. In (2) we indicate that the additional source term S_u in GDL and CL is named as Darcy's drag and defined by $S_u = -\frac{\mu}{K}\mathbf{u}$, where K is hydraulic permeability.

Species concentration equation. Water management is critical to achieve high performance for PEMFC. Therefore, without loss of generality, in order to focus on water management topics, we typically consider water as the only component in the following simplified species concentration equation. Water concentration equation in single gaseous phase is defined as follows with respect to concentration C

$$\nabla \cdot (\mathbf{u}C) = \nabla \cdot (D_g^{eff} \nabla C) + S_{H_2O}, \tag{3}$$

equation where $D_g^{eff} = \varepsilon^{1.5} D_{gas}$ is the effective water vapor diffusivity. The source term S_{H_2O} is given as follows.

$$S_{H_2O} = \begin{cases} -\nabla \cdot (\frac{n_d}{F}\mathbf{i}_e) - \frac{j}{2F} & \text{in cathode CL} \\ -\nabla \cdot (\frac{n_d}{F}\mathbf{i}_e) & \text{in anode CL} \\ 0 & \text{otherwise,} \end{cases} \tag{4}$$

where n_d, the electro-osmotic drag coefficient, is a constant value in our simulation. $\nabla \cdot \mathbf{i}_e = -j$ which is derived from the continuity equation of proton potential. $\mathbf{i}_e$ is the current density vector and j is the volumetric transfer current of the reaction (or transfer current density) defined by $j = j_1 - (j_1 - j_2)z/l_{cell}$. This is an approximation of transfer current density for our simplified single-phase PEMFC model due to the absence of proton and electron potentials [12].

1.2 Computational Domain and Boundary Conditions

The computational domain and its geometric sizes are schematically shown in Fig. 1 and Table 1.

For flow field (1), (2) and water concentration equation (3), the following boundary conditions are imposed:

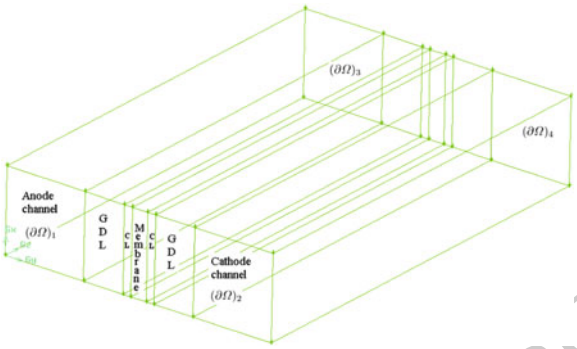

Fig. 1. Geometry of a single straight-channel PEMFC

Table 1. Physical coefficients and parameters

Parameter	Symbol	Parameter	Symbol
Anode/cathode channel width δ_{CH}	$6.180mm$	Anode/cathode GDL width δ_{GDL}	$0.235mm$
Anode/cathode CL width δ_{CL}	$0.010mm$	Membrane width δ_{mem}	$0.018mm$
Cell length l_{cell}	$70mm$	Cell depth h_{cell}	$6.360mm$
Porosity of membrane ε	0.26	Effective viscosity μ	$3.166\times10^{-5}kg/(m\cdot s)$
Porosity of GDL and CL ε	0.6	Water vapor diffusivity D_{gas}	$2.6\times10^{-5}m^2/s$
Vapor density ρ	$0.882\ kg/m^3$	Permeability of GDL and CL K	$2\times10^{-12}m^2$
Electro-osmotic drag coefficient n_d	1.5	Transfer current density j_1/j_2	$20000/10000A/m^2$

$$u_1 = u_2 = 0, u_3 = u_3|_{inlet}, C = C_{in} \quad \text{on inlet } (\partial\Omega)_1, (\partial\Omega)_2, \tag{5}$$

$$(PI - \mu\nabla\mathbf{u})\cdot\mathbf{n} = 0 \quad \text{on outlet } (\partial\Omega)_3, (\partial\Omega)_4, \tag{6}$$

$$u_1 = u_2 = u_3 = 0, \frac{\partial C}{\partial n} = 0 \quad \text{on other boundaries.} \tag{7}$$

2 Numerical Algorithm

2.1 Domain Decomposition Method and Weak Forms

First, we split the domain (Ω), shown in Fig. 1, to two overlapping subdomains: one is the anode and membrane (Ω_a), the other is the cathode and membrane (Ω_c). The interface between anode CL and membrane is denoted as $\mathscr{S}_a$, and the interface between cathode CL and membrane is denoted as $\mathscr{S}_c$. The classical overlapping Schwarz alternating method [13] is used in these two subdomains. Thus we are able to reformulate Eqs. (1)–(3) to two Dirichlet-type interfacial boundary value subproblems.

$$\text{(Problem A)}\begin{cases}\nabla\cdot(\rho\mathbf{u}_a)=0 & \text{in } \Omega_a\\ \frac{1}{\varepsilon^2}\nabla\cdot(\rho\mathbf{u}_a\mathbf{u_a})=-\nabla P_a+\nabla\cdot(\mu\nabla\mathbf{u}_a)-\frac{\mu}{K}\mathbf{u}_a & \text{in } \Omega_a\\ \nabla\cdot(\mathbf{u}_aC_a)=\nabla\cdot(D_g^{eff}\nabla C_a)+S_{H_2O} & \text{in } \Omega_a\\ u_{1,a}=u_{2,a}=0, u_{3,a}=u_3|_{inlet}, C_a=C_{a,in} & \text{on } (\partial\Omega)_1\\ (P_aI-\mu\nabla\mathbf{u_a})\cdot\mathbf{n}=0 & \text{on } (\partial\Omega)_3\\ C_a=C_c & \text{on } \mathscr{S}_c\\ u_{1,a}=u_{2,a}=u_{3,a}=0, \frac{\partial C}{\partial n}=0 & \text{on other boundaries.}\end{cases}$$

$$\text{(Problem C)}\begin{cases}\nabla\cdot(\rho\mathbf{u}_c)=0 & \text{in } \Omega_c\\ \frac{1}{\varepsilon^2}\nabla\cdot(\rho\mathbf{u}_c\mathbf{u_c})=-\nabla P_c+\nabla\cdot(\mu\nabla\mathbf{u}_c)-\frac{\mu}{K}\mathbf{u}_c & \text{in } \Omega_c\\ \nabla\cdot(\mathbf{u}_cC_c)=\nabla\cdot(D_g^{eff}\nabla C_c)+S_{H_2O} & \text{in } \Omega_c\\ u_{1,c}=u_{2,c}=0, u_{3,c}=u_3|_{inlet}, C_c=C_{c,in} & \text{on } (\partial\Omega)_2\\ (P_cI-\mu\nabla\mathbf{u_c})\cdot\mathbf{n}=0 & \text{on } (\partial\Omega)_4\\ C_c=C_a & \text{on } \mathscr{S}_a\\ u_{1,c}=u_{2,c}=u_{3,c}=0, \frac{\partial C}{\partial n}=0 & \text{on other boundaries.}\end{cases}$$

Considering various nonlinearities of equations, we particularly employ Picard's scheme to linearize the nonlinear source term. Define

$$V_a:=\{\mathbf{v}_a=(v_{1,a},v_{2,a},v_{3,a})^\top\in[H^1]^3\mid v_{1,a}|_{(\partial\Omega)_1}=v_{2,a}|_{(\partial\Omega)_1}=0, v_{3,a}|_{(\partial\Omega)_1}=u_{3,a}|_{inlet}\},$$
$$\widetilde{V}_a:=\{\mathbf{v}_a=(v_{1,a},v_{2,a},v_{3,a})^\top\in[H^1]^3\mid v_{1,a}|_{(\partial\Omega)_1}=v_{2,a}|_{(\partial\Omega)_1}=v_{3,a}|_{(\partial\Omega)_1}=0\},$$
$$Q_a:=\{w\in H^1\mid w|_{(\partial\Omega)_1}=C_{in,a}\text{ and }w|_{\mathscr{S}_c}=C_c\},\ \widetilde{Q}_a:=\{w\in H^1\mid w|_{(\partial\Omega)_1}=0\text{ and }w|_{\mathscr{S}_c}=0\},$$
$$P_a:=L^2(\Omega_a).$$

Then for any $(\mathbf{v}_a,q_a,w_a)\in\widetilde{V}_a\times P_a\times\widetilde{Q}_a$, find $(\mathbf{u}_a^{k+1},P_a^{k+1},C_a^{k+1})\in V_a\times P_a\times Q_a$, such that

$$\begin{cases}(\mu\nabla\mathbf{u}_a^{k+1},\nabla\mathbf{v}_a)_{\Omega_a}+(\frac{\rho}{\varepsilon^2}\nabla\mathbf{u}_a^k\mathbf{u}_a^{k+1},\mathbf{v}_a)_{\Omega_a}-(P_a^{k+1},\nabla\mathbf{v}_a)_{\Omega_a}+(\frac{\mu}{K}\mathbf{u}_a^{k+1},\mathbf{v}_a)_{\Omega_a}=0\\ (\nabla\mathbf{u}_a^{k+1},q_a)_{\Omega_a}=0\\ (D_g^{eff}\nabla C_a^{k+1},\nabla w_a)_{\Omega_a}+(\nabla\cdot(\mathbf{u}_a^kC_a),w_a)_{\Omega_a}=(S_{H_2O},w_a)_{\Omega_a},\end{cases}\tag{8}$$

which $(\cdot,\cdot)_{\Omega_i}$ stands for the L^2 inner product in Ω_i. And in subdomain Ω_c, we have the same weak form with (8).

2.2 An Overlapping Domain Decomposition Algorithm

Firstly, the subdomains Ω_a and Ω_c are partitioned into cuboids independently, which implies that the grids are local structured in anode and cathode. Define a partition $\mathscr{T}_{h_i}$ in Ω_i (i,j represent a or c), and $\Sigma_{i,j}$ is the set of mesh points of $\mathscr{T}_{h_i}$ on $\mathscr{S}_j$.

To discretize weak form (8), we introduce the finite element space $V_{h_i}\times P_{h_i}\subseteq V_i\times P_i$ on $\mathscr{T}_{h_i}$, where $V_{h_i}\times P_{h_i}$ denotes the $Q2Q1$ (triquadratic velocity and trilinear pressure) finite element spaces. Q_{h_a} denotes the triquadratic finite element space for water concentration whose members equal f_a on $\mathscr{S}_c$, where f_a represents the values of points in the sets of $\Sigma_{a,c}$, which are obtained from the previous alternating step C^k

by lagrange interpolation. Moreover, let $\widetilde{Q}_{h_a} \subseteq \widetilde{Q}_a$ be the triquadratic finite element space and $\widetilde{V}_{h_a} \subseteq \widetilde{V}_a$ be the triquadratic finite element space. In subdomain Ω_c, Q_{h_c} and $\widetilde{V}_{h_c}$ are defined in the same ways.

For flow and water concentration equations, we introduce the following combined finite element-upwind finite volume schemes [11].

For any given $(\mathbf{u}_{h_i}^k, P_{h_i}^k, C_{h_i}^k) \in V_{h_i} \times P_{h_i} \times Q_{h_i}$ $(k = 0, 1, 2, \ldots)$, find $(\mathbf{u}_{h_i}^{k+1}, P_{h_i}^{k+1}, C_{h_i}^{k+1}) \in V_{h_i} \times P_{h_i} \times Q_{h_i} (k = 0, 1, 2, \ldots)$, such that

$$(\mu \nabla \mathbf{u}_{h_i}^{k+1}, \nabla \mathbf{v}_{h_i})_{\Omega_i} + (\frac{\rho}{\varepsilon^2} \nabla \mathbf{u}_{h_i}^k \mathbf{u}_{h_i}^{k+1}, \mathbf{v}_{h_i})_{\Omega_i} - (P_{h_i}^{k+1}, \nabla \mathbf{v}_{h_i})_{\Omega_i} + (\frac{\mu}{K} \mathbf{u}_{h_i}^{k+1}, \mathbf{v}_{h_i})_{\Omega_i} = 0$$
$$(\nabla \mathbf{u}_{h_i}^{k+1}, q_{h_i})_{\Omega_i} = 0 \quad \forall (\mathbf{v}_{h_i}, q_{h_i}) \in \widetilde{V}_{h_i} \times P_{h_i}, \quad (9)$$

$$(D_g^{eff} \nabla C_{h_i}^{k+1}, \nabla w_{h_i})_{\Omega_i} + (\nabla \cdot (\mathbf{u}_{h_i}^{k+1} C_{h_i}^{k+1}), w_{h_i})_{\Omega_i} + \delta(h_i) \mathbf{u}_{h_i}^{k+1} \cdot (\nabla C_{h_i}^{k+1}, \nabla w_{h_i})_{\Omega_i}$$
$$= (S_{H_2O}, w_{h_i})_{\Omega_i} \quad \forall w_{h_i} \in \widetilde{Q}_{h_i}, (10)$$

where the last term in the left hand side of (10) is a stabilizing term, derived from streamline-diffusion scheme [3, 6–8]. Basically we hold $\delta(h) = Ch$, C is a certain constant parameter, which is chosen artificially with least possible on the premise of optimal stability. Usually starting with small ones, we gradually increase the value of C and compute the corresponding finite element equation (10) until gained numerical solutions are not oscillating any more in convection-dominated gas channel.

Now, we are in position to describe the overlapping domain decomposition algorithm with the finite element discretizations.

Algorithm: Given $\mathbf{u}_h^0, C_h^0$, the following procedures are successively executed $(k > 0)$:

Step 1. Solve (9) in Ω_a and Ω_c for $(\mathbf{u}_{h_i}^{k+1}, P_{h_i}^{k+1})$, respectively, until

$$\|\mathbf{u}_{h_i}^{k+1} - \mathbf{u}_{h_i}^k\|_{L^2(\Omega_i)} + \|P_{h_i}^{k+1} - P_{h_i}^k\|_{L^2(\Omega_i)} < \text{tolerance}. \quad (11)$$

Step 2. Solve (10) for $C_{h_a}^{k+1}$, and construct the finite element space $\widetilde{Q}_{h_c}$ for Ω_c.

Step 3. Solve (10) for $C_{h_c}^{k+1}$, and construct the finite element space $\widetilde{Q}_{h_a}$ for Ω_a.

Step 4. Compute the following stopping criteria:

$$\|C_{h_a}^{k+1} - C_{h_a}^k\|_{L^2(\Omega_a)} < \text{tolerance}. \quad (12)$$

If yes, then numerical computation is complete. Otherwise, go back to the step 2 and continue.

3 Numerical Results

In this section, we will carry out the following numerical experiments which indicate that our methods are effective to deal with the non-matching grids, see Fig. 2 for example, in the simulation of the PEMFC. The velocity $u_3|_{inlet}$ is defined as a paraboloidal-like function given in (13).

$$u_3|_{inlet} = \begin{cases} 0.2\sin\frac{x\pi}{\delta_{CH}}\sin\frac{y\pi}{\delta_{CH}} & \text{on anode inlet } (\partial\Omega)_1 \\ 0.3\sin\frac{x\pi}{\delta_{CH}}\sin\frac{(y-l_{add})\pi}{\delta_{CH}} & \text{on cathode inlet } (\partial\Omega)_2 \end{cases}, \tag{13}$$

where $l_{add} = \delta_{CH} + \delta_{GDL} + \delta_{CL} + \delta_{mem}$.

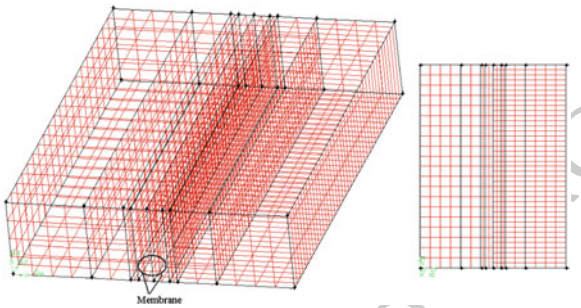

Fig. 2. An example of non-matching grids

Figures 3 and 4 show the velocity field in anode and cathode of fuel cell at the face of $x = 3.18$ mm with this two method. As expected, there is a large difference in the velocity scale between the porous media and the open channel. The velocity in porous GDL is at least two orders of magnitude smaller than that in the open gas channel, indicating that gas diffusion is the dominant transport mechanism in porous GDL. Porous CL has a smaller velocity than GDL due to the inferior diffusion ability.

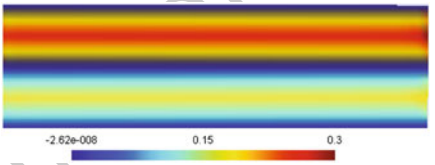

Fig. 3. Velocity with DDM

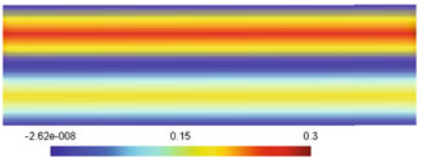

Fig. 4. Velocity with single domain

Figure 5 displays the water concentration distribution, presenting in the phase of water vapor, in anode and cathode. As shown in the figure, significant variations are displayed in both anode and cathode; in the porous media there is an increased water vapor concentration along the channel.

In order to verify the correctness of our numerical solutions, we compute the relative error of mass balance in terms of the numerical fluxes at the inlet and outlet.

$$\text{mass balance error} = \frac{|\int_{(\partial\Omega)_{outlet}} Cu_3 dS - \int_{(\partial\Omega)_{inlet}} C_{in}u_3|_{inlet} dS - \int_{\Omega} S_{H_2O} dV|}{\int_{(\partial\Omega)_{inlet}} C_{in}u_3|_{inlet} dS.} \tag{14}$$

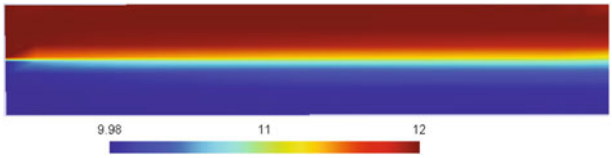

Fig. 5. Distributions of water concentration with DDM

The tolerance of our stopping criteria (12) for Schwarz alternating iteration is 10^{-20}. By plugging the assigned and the computed concentration C as well as horizontal velocity u_3 in Eq. (14), we attain a convergent mass balance error for our numerical solutions along with the continuously refining grids, shown in Table 2. A more accurate mass balance error is attained for the numerical solutions with DDM.

Table 2. Convergent mass balance error for with different grids

	Grids	Unknowns	Error with DDM	Error with single domain
Mesh1	720	36260	9.731×10^{-3}	8.112×10^{-3}
Mesh2	1440	58660	8.338×10^{-3}	6.909×10^{-3}
Mesh3	2880	115884	3.774×10^{-3}	2.233×10^{-3}
Mesh4	3600	139840	1.528×10^{-3}	Overflow

4 Conclusions and Future Work

In this paper, a simplified single-phase 3D steady PEMFC model is introduced by a modified Navier-Stokes equations for mass and momentum, and a conservation equation for water concentration. Based on the combined finite element-upwind finite volume methods and the overlapping domain decomposition method, a new discretization scheme is designed and implemented for the PEMFC model. Numerical experiments demonstrate that our methods are effective to deal with the non-matching grids and obtain a relatively accurate numerical solution with low mass balance error. The derived discretization scheme will be also studied for two-phase unsteady and/or fuel cell stack model in our further work.

Acknowledgments The support from the NFSC (No.11101311) is fully acknowledged. Ziping Huang also acknowledge "Applied Mathematics Chair Fund of China-German College" (0900101021). Pengtao Sun is supported by NSF Grant DMS-0913757.

Bibliography

[1] R. E. Bank and J. Xu. Asymptotically exact a posteriori error estimators, part I: grids with superconvergence. *SIAM Journal on Numerical Analysis*, 41:2294–2312, 2003.

[2] C. H Cheng and H. H Linb. Numerical analysis of effects of flow channel size on reactant transport in a proton exchange membrane fuel cell stack. *Journal of Power Sources*, 194:349–359, 2009.

[3] M. Feistauer and J. Felcman. On the convergence of a combined finite volume-finite element for nonlinear convection–diffusion problems. *Numerical Methods for Partial Differential Equations*, 13:163–190, 1997.

[4] Y. Q. Huang. Superconvergence for quadratic triangular finite elements on mildly structured grids. *Mathematics of computation*, 77:1253–1268, 2008.

[5] Hyunchul Ju A single-phase, non-isothermal model for pem fuel cells. *International Journal of Heat and Mass Transfer*, 48:1303–1315, 2005.

[6] Dietmar Kroner and Mirko Ohlbefger. A posteriori error estimates for upwind finite volume schemes for nonlinear conservation laws in multi-dimensions. *Numerische Mathematik*, 69:25–39, 2000.

[7] Dietmar Kroner and Mirko Rokyta. Convergence of upwind finite volume schemes for scalar conservation laws in two dimensions. *SIAM Journal on Numerical Analysis*, 31:324–343, 1994.

[8] Dietmar Kroner. Convergence of higher order upwind finite volume schemes on unstructured grids for scalar conservation laws in several space dimensions. *Mathematics of Computation*, 71:527–560, 1995.

[9] Atul Kumar and Ramana G. Reddy. Effect of channel dimensions and shape in the flow-field distributor on the performance of polymer electrolyte membrane fuel cells. *Journal of Power Sources*, 113:11–18, 2003.

[10] S. Shimpalee and J.W. Van Zee. Numerical studies on rib and channel dimension of flow-field on PEMFC performance. *International Journal of Hydrogen Energy*, 32:842–856, 2007.

[11] Pengtao Sun, Guangri Xue, Chaoyang Wang, and Jinchao Xu. A domain decomposition method for two-phase transport model in the cathode of a polymer electrolyte fuel cel. *Journal of Computational Physics*, 228:6016–6036, 2009.

[12] Pengtao Sun, Guangri Xue, Chaoyang Wang, and Jinchao Xu. Fast numerical simulation of two-phase transport model in the cathode of a polymer electrolyte fuel cell. *Communications in Computational Physics*, 6:49–71, 2009.

[13] Andrea Toselli and Olof B.Widlund. *Domain decomposition methods - algorithms and theory*. Springer, New York, 2005.

[14] L. B. Wahlbin. *Superconvergence in Galerkin Finite Element Methods*. Springer, Berlin, 1995.

[15] C. Y. Wang. Computational fluid dynamics modeling of proton exchange membrane fuel cells. *Journal of the Electrochemical Society*, 147:4485–4493, 2000.

[16] C. Y. Wang. Fundamental models for fuel cell engineering. *Journal of the Electrochemical Society*, 104:4727–4766, 2004.